Smart Structures and Systems, *Vol. 15, No. 6 (2015) 1521-1542*
DOI: http://dx.doi.org/10.12989/sss.2015.15.6.1521

Experimental analyses of dynamical systems involving shape memory alloys

Søren Enemark[1a], Marcelo A. Savi[*2] and Ilmar F. Santos[1b]

[1]*Technical University of Denmark, Department of Mechanical Engineering, DK-2800 Kgs. Lyngby, Denmark*
[2]*Universidade Federal do Rio de Janeiro, COPPE – Department of Mechanical Engineering, 21.941.972 – Rio de Janeiro – RJ – Brazil, P.O. Box 68.503*

(Received September 5, 2013, Revised April 20, 2014, Accepted May 16, 2014)

Abstract. The use of shape memory alloys (SMAs) in dynamical systems has an increasing importance in engineering especially due to their capacity to provide vibration reductions. In this regard, experimental tests are essential in order to show all potentialities of this kind of systems. In this work, SMA springs are incorporated in a dynamical system that consists of a one degree of freedom oscillator connected to a linear spring and a mass, which is also connected to the SMA spring. Two types of springs are investigated defining two distinct systems: a pseudoelastic and a shape memory system. The characterisation of the springs is evaluated by considering differential calorimetry scanning tests and also force-displacement tests at different temperatures. Free and forced vibration experiments are made in order to investigate the dynamical behaviour of the systems. For both systems, it is observed the capability of changing the equilibrium position due to phase transformations leading to hysteretic behaviour, or due to temperature changes which also induce phase transformations and therefore, change in stiffness. Both situations are investigated by promoting temperature changes and also pre-tension of the springs. This article shows several experimental tests that allow one to obtain a general comprehension of the dynamical behaviour of SMA systems. Results show the general thermo-mechanical behaviour of SMA dynamical systems and the obtained conclusions can be applied in distinct situations as in rotor-bearing systems.

Keywords: shape memory alloys; dynamic systems; stiffness changes; phase transformation; experimental tests

1. Introduction

Smart materials present a coupling between different fields, e.g., mechanical, electrical and magnetic, and because of that, they are of great interest in several engineering applications. This kind of coupling provides special behaviours, properties and capabilities compared to conventional materials. Systems built with smart materials have adaptive behaviour that may change with environmental modifications. Shape memory alloys (SMAs) belong to the smart materials family and the driving force of the remarkable properties is their phase transformations that can be

∗Corresponding author, Professor, E-mail: savi@mecanica.ufrj.br
[a] Ph.D. Student, E-mail: soene@mek.dtu.dk
[b] Professor, E-mail: ifs@mek.dtu.dk

Copyright © 2015 Techno-Press, Ltd.
http://www.techno-press.org/?journal=sss&subpage=8 ISSN: 1738-1584 (Print), 1738-1991 (Online)

induced either by stress or temperature fields.

Several researches are dedicated to characterise, model and explore potential applications of SMAs. In general, one should say that applications can vary from different fields of human knowledge including civil engineering, aerospace, robotics, biomedical, oil and energy industries. Machado and Savi (2003), Paiva and Savi (2006) and Lagoudas (2008) presented a general overview of SMA applications.

Concerning dynamical applications, SMAs have been used for different purposes. Vibration reduction is one of these possibilities where phase transformations can be exploited in order to confer adaptive characteristics to the system. In brief, it is possible to say that hysteretic behaviour together with stiffness changes due to temperature variations can confer system changes that alter dynamical responses in a desirable way. Adaptive vibration absorbers are one of the possibilities related to this kind of application (Savi *et al*. 2011, Williams *et al*. 2002). Lees *et al.* (2007) included SMA wires in a rotor-bearing system and changed their stiffness with temperature variations which enhanced the performance when passing through critical speeds. This approach has been suggested several times in literature since Nagaya *et al*. (1987). Dhanalakshmi *et al.* (2010) used active temperature controlled SMA wires as actuators to dampen vibrations of a cantilevered beam, and the investigation was carried out both theoretically and experimentally. In civil engineering SMAs are used for mitigating earthquakes on e.g., heritage structures and strayed bridges (Casciati and Hamdaoui 2008, Torra *et al*. 2009, Alam *et al*. 2008, Ozbulut *et al*. 2011). The SMAs are mostly only exposed to a few cycles (order of 100). Nevertheless, the evolution of e.g., the dissipative capabilities over the lifetime is of concern (Torra *et al*. 2009, Casciati and Marzi 2010). It is well-known that SMAs have a relatively short lifetime in terms of cycles especially when subjected to large deformations, where the lifetime is in the order of 10^3 cycles, where also the dissipative characteristics of the SMAs change drastically. In these investigations the lifetime aspects of the smart springs have not been considered. Another interesting application of SMA dynamics is related to its use in impact systems. The main idea is to exploit the high dissipation capacity of SMAs in order to dissipate energy. Dos Santos and Savi (2009) and Sitnikova *et al*. (2010) discussed one degree of freedom oscillators with a discontinuous support built with an SMA element. This idea is useful in dynamical rotor systems where impacts between the shaft and the bearing are common. Silva *et al*. (2013) investigated this phenomenon numerically, where the discontinuous rotor support included SMA elements.

Dynamical response of SMA systems is very complex presenting periodic, quasi-periodic and chaotic behaviours. Literature presented several research efforts dealing with the complex non-linear dynamics of SMA systems. Some examples of this profusion can be found in the following references: Savi *et al.* (2008), Machado *et al.* (2009), Bernardini and Rega (2005), Savi and Pacheco (2002a, b), Machado and Savi (2003). Nevertheless, there is a lack of experimental work related to SMA dynamical systems. Aguiar *et al.* (2013) investigated an experimental SMA system excited with a shaker showing the idea of vibration reduction. Sitnikova *et al.* (2012) continued the work on a discontinuous SMA support experimentally, and confirmed periodic, quasi-periodic and chaotic behaviours.

SMAs are also used as actuators for controlling geometries, e.g., the size of the intake for a jet engine Song *et al*. (2011). Here a machine element solution involving SMAs was chosen, because it is simpler and more compact than conventional solutions.

The objective of this research effort is to investigate the non-linear dynamics of a one degree of freedom SMA oscillator, both in free and forced modes. The dynamical system consists of a cart with a mass connected to a linear spring and an SMA spring in pre-tension. The system is excited

by a DC motor and variables are monitored by motion sensors. Two different types of SMA helical springs are employed: a pseudoelastic, where the austenitic phase is stable at room temperature; and a shape memory, where the martensitic phase is stable at room temperature.

Experiments are split into three parts: characterisation of the SMA springs; free vibration tests; and forced vibration tests. The influence of temperature variations are of special interest and the main goal is to perform a qualitative analysis of the SMA dynamical behaviour. The influence of temperature in SMA is well quantified in literature for either quasi-static temperature, stress or strain conditions (Lagoudas 2008, Ozbulut *et al*. 2011). However, in this work stress, strain and temperature changes are simultaneous and the dynamic responses are under investigation, and this is not well documented in literature. The original contribution of this work is the experimental observation of several dynamical behaviours related to SMA systems; especially the thorough investigation of the moving equilibrium position as consequence of changing initial martensitic volume fraction and temperature condition. The investigations are aimed towards application of SMAs in dynamical systems such as in rotor-bearing systems to obtain changing critical speeds, to obtain a self-alignment mechanism, or as elements in a secondary support bearings for reducing the severity of impacts or whirl. Before designing such systems, a general understanding of the SMAs' dynamical behaviour is necessary.

2. Shape memory alloy experimental system

Shape memory alloys are characterised by several thermo-mechanical behaviours that include pseudoelasticity, shape memory effect, phase transformation due to temperature variations, among others. Many alloys may present these effects however, the Nickel-Titanium alloys combine these effects with good mechanical properties being widely employed in engineering applications. Phase transformations induced either by stress or temperature are the driving force for the unique properties of SMAs. For a basic understanding of SMAs, the reader is referred to e.g., Paiva and Savi (2006), Lagoudas (2008), Aguiar *et al.* (2010), Ozbulut *et al*. (2011).

2.1 Experimental set-up

The experimental set-up is a one degree of freedom SMA oscillator that consists of a cart with a mass connected to a linear spring and an SMA spring. The system is excited by a 12 V DC motor and variables are monitored by motion sensors. Two different types of SMA helical springs are employed: a pseudoelastic (PE), where the austenitic phase is stable at room temperature; and a shape memory effect (SM), where the martensitic phase is stable at room temperature. Fig. 1 presents a system picture while a sketch of the system components is shown in Fig. 2. The experimental set-up is monitored by two rotary motion sensors (PASCO encoder CI-6538 with 1440 orifices and a precision of 0.25°): one for measuring the time depending input displacement x and one for the cart movement y. A force sensor is also employed to monitor the SMA spring force at point C, see Fig. 2. A power supply is coupled to the ends of the SMA spring in order to promote heating by Joule effect. Since the system response is highly temperature dependent, changes in electrical current induce different system behaviours. The temperature in itself is not measured, but since there is a direct relationship between electrical power and temperature it is possible to infer the temperature changes. Moreover, a DC motor is employed to provide sinusoidal excitation to the system. Nylon thread is used for connecting the different elements. The

thread is several orders of magnitude stiffer than the smart and linear springs. Different values of masses are used in the two systems. This variation is adopted in order to choose proper values of resonance conditions. Geometric properties of the SMA springs, the properties of the other system components as well as characteristic quantities of the systems are shown in Table 1.

This SMA oscillator may be considered as an archetypal model of a general SMA system. The scaling factor is an important issue to be addressed to convert system responses of this archetypal model and a real system. One of the essential issues related to that is the rate dependent behaviour. Although the martensitic phase transformation is rate independent, SMA systems have rate dependent behaviour due to thermal aspects. Therefore, environmental convection can dramatically change in larger systems, altering the thermo-mechanical aspects of the SMA. Nevertheless, the archetypal model describes the qualitative behaviour of SMA systems, providing useful results.

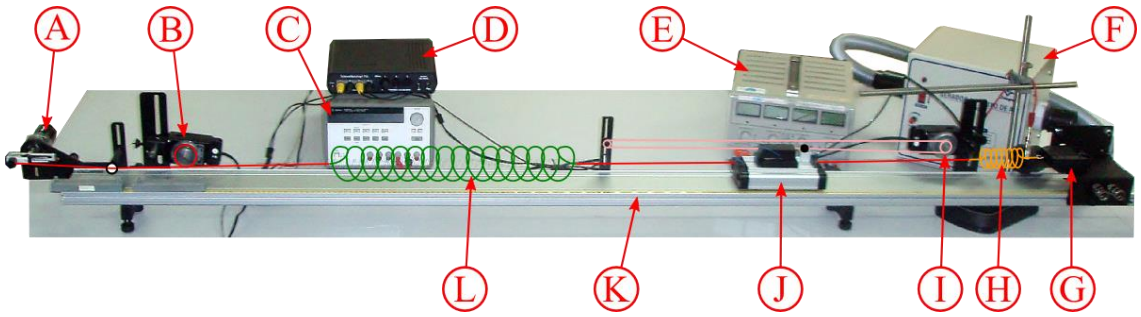

Fig. 1 Experimental set-up. (A) PASCO oscillator, (B) PASCO rotary motion sensor for measuring the input displacement, (C) power supply to oscillator, (D) PASCO receiver connected to sensors and computer, (E) power supply for heating the PE or SM spring, (F) blower for cooling the PE or SM spring, (G) PASCO force sensor for measuring the spring force, (H) SM or PE spring, (I) PASCO rotary motion sensor for measuring the displacement of the cart, (J) PASCO cart with masses, (K) PASCO horizontal slide, (L) linear spring. Between the oscillator, springs, cart and force sensor nylon threads connect the elements

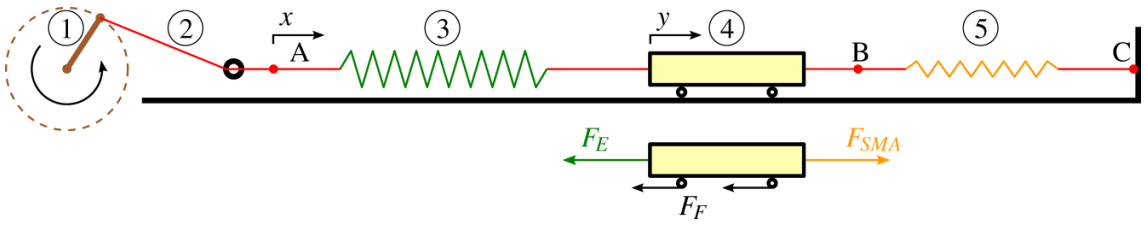

Fig. 2 Sketch of mechanical components in the experimental set-up. To the left is an oscillator (brown, 1) pulling a thread (red, 2). The linear spring (green, 3) is connected to the cart (yellow, 4). On the right side of the cart is the smart spring, either the PE or SM spring (orange, 5). The displacement of the oscillating part of the thread, the input x, is measured at point A. The displacement of the cart, the output y, is measured at point B. At point C the thread force is measured, equalling the smart spring force. F_{SMA} is the smart spring force, F_E is the linear elastic spring force, and F_F is the friction force from the wheels of the cart

Table 1 Data of experimental set-ups as well as characteristic quantities
*) For pre-tension of smart spring more than 60 mm

System	**PE**	**SM**
Smart spring		
Wire diameter d [mm]	0.50	0.70
Coil diameter D [mm]	5.6	6.4
Initial length l_0 [mm]	65	19
Number of coils N	36	21
Initial stiffness k_0 [N/m]	20	200*
Cart		
Mass m [g]	770	1270
Linear steel spring		
Stiffness k_l [N/m]	3.2	6.7
Characteristic quantities (besides l_0 and k_0)		
Spring force $F_0 = k_0 l_0$ [N]	1.3	1.3
Frequency $\omega_0 = \frac{1}{2\pi}\sqrt{(k_0 + k_l)m^{-1}}$ [Hz]	0.87	2.03

Note that simple models can help the scaling factor regarding helical springs. Aguiar *et al.* (2010) described the thermo-mechanical response of helical springs and these results can be employed to design systems in different scales.

3. Pseudoelastic system

This section presents results related to the PE system where a pseudoelastic spring is employed. Initially, the spring characterisation is presented. Afterwards, free and forced vibrations are investigated.

3.1 Spring characterisation

This section presents the characterisation of the PE spring used in the experimental set-up. This is done by using a DSC test and also by considering force-displacement curves. Fig. 3 and Table 2 present results of the DSC test, showing the amount of heat per mass necessary to maintain a constant temperature rate during either heating or cooling for a small SMA specimen. At a peak or valley, phase transformations happen. The beginning and finish temperatures of a transformation is defined as the temperature, where the steepest tangent during transformation and the tangent

before/after the transformation intersect. An example of the tangential fit is seen in the Fig. 3 in the heating process. This definition is used because the beginning and finish of the transformations are smooth as can be seen in the DSC results in the figure. Note that, at room temperature (25℃) the PE spring is stable at the austenitic state since the austenitic finish temperature A_f is lower than this.

The force-displacement curves of the PE spring are now focused on. This experimental test is done by uncoupling the linear spring of the oscillator from the system shown in Fig. 2 and a chosen displacement path is induced to the cart. The movement of the cart and the PE spring force are both measured. Experimental tests are done in different temperatures by inducing distinct values of electric current. Results are shown in Fig. 4. The movement in Fig. 4(a) (room temperature) follows the sequence: O–A–B–C–O–A–B–C–D–E–D–E–D–O referring to the letters in the figure. At the beginning of the process the spring in the austenitic phase. The transformation into detwinned martensite starts around point A. The reverse transformation to austenite starts around point C on the path from point B. It should be noted that point A is at a lower force than point C. It indicates that forward and reverse transformations from austenite to detwinned martensite are overlapping in the temperature-stress phase plane. It is important to note that the system does not reach a complete phase transformation to detwinned martensite.

It is important to highlight that this spring is subjected to large displacements, reaching more than four times the original length. Therefore, complex stress distributions can be induced, causing non-homogeneous phase transformations. The slopes of the curves a and b in Fig. 4(a) reveal that austenitic phase a has a slope of approximately 20 N/m (k_0) while slope b is around 31 N/m ($1.6k_0$), and here the spring consists of both austenite and detwinned martensite. The stiffness is proportional to the shear modulus, when the spring is only subjected to shear stress and no phase transformation happens (Aguiar *et al*. 2010). However, at large strains in the spring normal stresses may be induced resulting in a stiffening effect (Phillips and Costello 1972). This explains why the stiffness b is higher than stiffness a even though the austenitic shear modulus (and also Young's modulus) is higher than the martensitic.

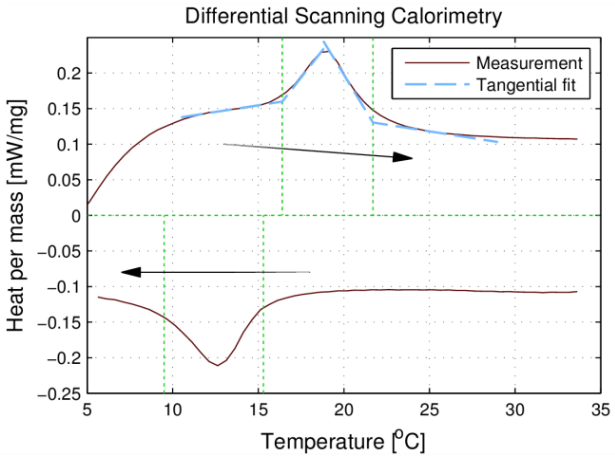

Fig. 3 The resulting graph from a DSC test for the PEspring

Table 2 Transformation temperatures forthe PE spring extracted from theDSC test

M_f [℃]	9.5
M_s [℃]	15.3
A_s [℃]	16.4
A_f [℃]	21.7

During phase transformation (forward A–B, and reverse C–D) the slopes are 10 N/m ($0.5k_0$). This means that the average stiffness can vary from 10 N/m during phase transformations to 31 N/m in some elastic phases, which is a factor of three, for the same spring at room temperature. The dissipation due to hysteresis is another important characteristic of the PE spring. Note that the increase of displacement tends to be related to the increase of dissipation due to larger hysteresis loop. When the spring is subjected to different amounts of electric current the temperature rises. Basically, four values of electric current are considered: 0, 0.4, 0.6 and 1 A. It is roughly estimated that 1.0 A is equivalent to 80℃. The increase in temperature induces the movement in force of the hysteresis loop as can be observed in Fig. 4(b). The austenitic slope of the three heated springs are almost equal, the difference lies in at what force the phase transformation starts. When the electric current is 1.0 A, there is almost no phase transformation taking place, and the force-displacement behaviour is almost linear. The hysteretic effect is also smaller at the two other heated cases. This indicates that not only the average stiffness but also the dissipation effect is changed when temperature is altered.

3.2 Free vibration

The free vibration analysis considers the set-up shown in Fig. 1 by implying that the DC motor is turned off. Temperature influence is investigated during the tests.

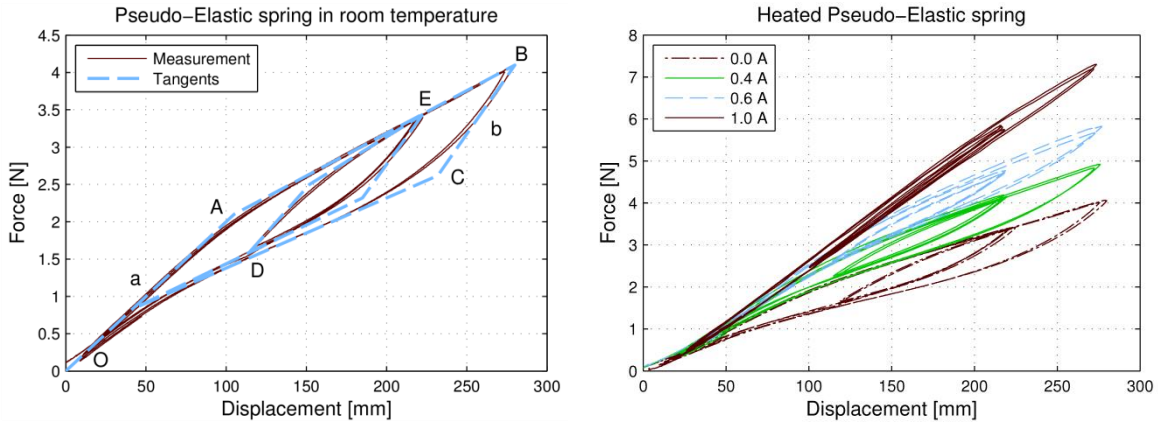

(a) (b)

Fig. 4 Force-displacement behaviour of the PE spring

3.2.1 Constant temperature

Initially, let us consider constant temperature tests. Our analysis starts by assuming a test that is done at room temperature. An equilibrium position is a point in y, where the sum of forces acting on the cart vanishes. Therefore, it should be a proper balance between the elastic spring force F_E and the SMA spring force, $F_{SMA}=F_{PE}$, namely $F_E=F_{PE}$. Fig. 5 shows the force-displacement curves for both springs of this system. The places where the two different lines intersect establish a proper balance between the spring forces, representing equilibrium positions. Note that the lines are crossing four times, but one could imagine an infinite number of possibilities along the dash-dotted line, for values of y smaller than approximately 25 mm in this case, since this is the maximum force considered for the PE spring. It should be pointed out that there is only one equilibrium point at any instant in time or cart position, but the equilibrium is able to move along the line.

Free vibration tests are done by releasing the cart from a range of positions, measuring the displacement and the PE force until the cart is at rest. Both the linear spring and the PE spring are attached to the cart.

This test is done by considering three levels of pre-tension. The definition of this value is done by changing the length of the thread between the linear spring and the cart. Furthermore, a test is done with the PE spring heated with 1.0 A of electric current.

In Fig. 6 seven of the tests for a single pre-stress level at room temperature are shown, highlighting the starting and terminal points. The position of the equilibrium point is determined by the initial position and the amount of detwinned martensite as initial condition.

The time series in Fig. 7 shows that the vibration amplitudes decay rapidly within a few seconds. The decay in amplitude in the last 4-5 cycles has an exponential form, where the oscillations are small. The exponential function was fitted from the experimental data. In the last 4-5 cycles the dissipation is not caused by hysteretic effects from the PE spring, but rather other dissipative mechanisms in the system. Because of the exponential decay characteristic these effects are equivalent to viscous dissipation. Nevertheless, in the first 2 cycles the dissipation is larger, as it can be seen in the marked circles, which indicates that the hysteretic phase transformations also take place in addition to the other dissipative effects. From Fig. 7 it is also possible to conclude that the system oscillation period in the first couple of cycles is around 25% larger than in the last cycles, i.e., 1.3 s and 1.0 s respectively. This indicates an increase in stiffness as consequence of a decrease in oscillation amplitude and therefore deformation of the spring. This is in good agreement with the other experiments showing that the average stiffness is smaller in loops with phase transformations than in loops without.

The starting and terminal points of each test are now highlighted in Fig. 8. For the three values of pre-stresses, the starting point is varied in a range of 170 mm ($2.6l_0$), and this gives a variation of 30 mm ($0.5l_0$) to the equilibrium point positions. It is seen that if the starting point is far away from the equilibrium point (high distance from the starting point to the red stippled line) the equilibrium point is almost constant for the two low levels of pre-stresses. On the other hand, as the distance decreases the y-value of the equilibrium point increases. A high y-value corresponds to a low level of martensite. These results show that the equilibrium position depends on both the starting position and the amount of martensitic phase induced by the pre-stress level.

Results of the high temperature test are shown in Fig. 9. It is seen that the PE spring force is almost linear indicating that phase transformations are not occurring even though the displacements are large. As a consequence, there is a smaller amount of dissipation. Due to the linear behaviour of the PE spring, the equilibrium position is almost constant. Furthermore, the

equilibrium position has a larger value (y=80 mm) when compared with the low temperature results ($y \in [-25;50]$ mm) because of the higher average PE stiffness (36 N/m=1.8k_0). This change due to temperature will be further investigated in the following sections.

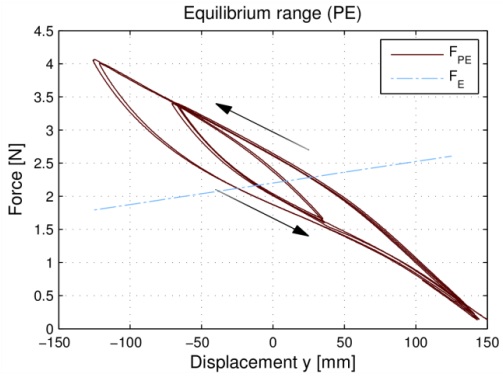

Fig. 5 Illustration of the range of equilibrium positions for the system with the PE spring. The arrows indicate the loading nature of the loop

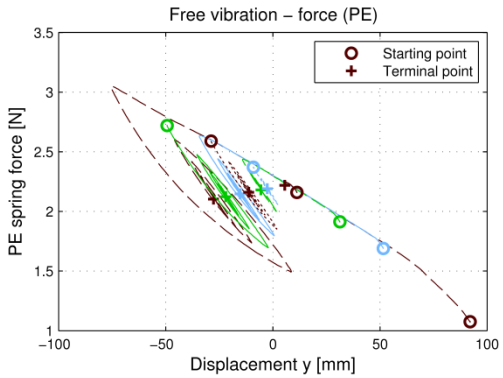

Fig. 6 PE spring force of seven free vibration tests with a pre-stress level of 2.3N

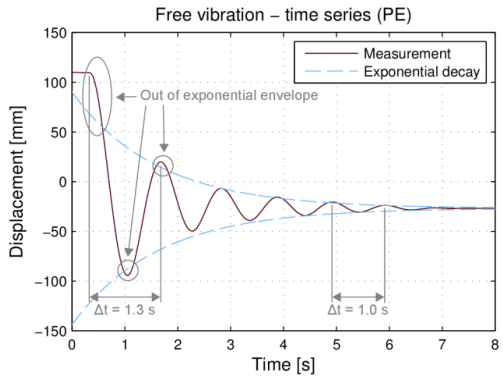

Fig. 7 Free vibration test with the PE spring at a pre-stress level of 2.3 N (1.8F_0)

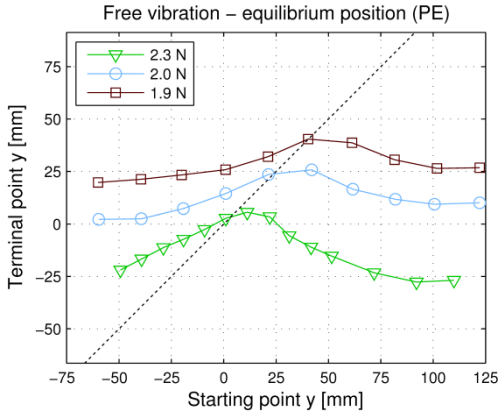

Fig. 8 The variation of the equilibrium position for the system with the PE spring and three levels of pre-stress. The starting point and terminal point are equal along the dotted line

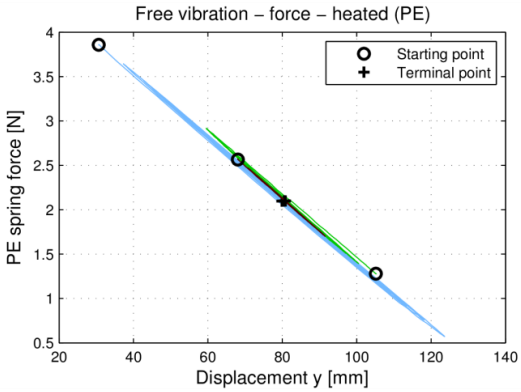

Fig. 9 Force and state space of the free vibration tests with the PE spring heated with 1.0A and a pre-stress level of 2.1N

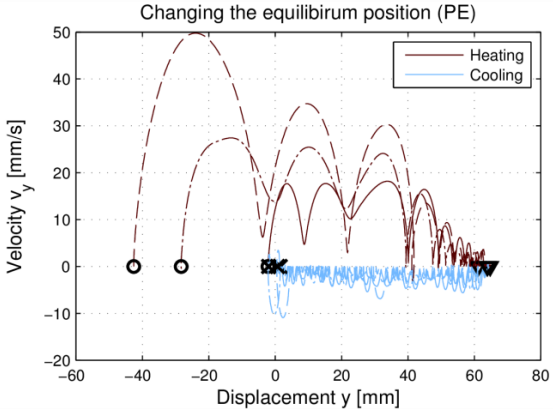

Fig. 10 The equilibrium position is change due to temperature changes. The three different experiments start at ○, go to ▽and end at ×

3.2.2 Varying temperature

This section deals with tests where the cart is released at one of its equilibrium positions, evaluating the influence of temperature changes. After a heating process, the spring is cooled down again simply by natural convection. An indicative time constant for the heating process is 7 s, whereas for the cooling it is 15 s. The test is done with three different starting positions. Results are shown in Fig. 10. By heating the PE spring in tension, phase transformation to austenite is taking place. The equilibrium position at this state is independent of the starting point, as the triangles are placed on top of each other. The movement to the new equilibrium position happens in a jagged fashion and it is not smooth. This is believed to be caused by the nature of the phase transformations. When the springs are cooled down, the cart moves backwards, but only to a minimum amount of detwinned martensite, which is also independent of the starting point. This motion is very slow, due to the slow cooling process. Again the movement is not smooth. These results show that it is possible to get to the same position, a zero position, no matter what prior activity the spring has been exposed to simply by heating and cooling the spring. Note that the distance between the equilibrium positions are larger compared with the initial length of the spring, see Table 1. The PE spring force is higher at $\bigtriangledown$(2.7 N = 2.1F_0) than at × (2.4 N = 1.8F_0) even though the spring is more elongated at ×.

3.3 Forced vibration

After the free vibration analysis, the system is now forced by the DC motor rotating a lever pulling a thread, see Fig. 2. The input is therefore a displacement against time. The difference in input and output displacements determines the actuation force from the linear spring. Different forcing parameters, such as frequency and displacement amplitude, and temperature are treated. Initially, a frequency response is performed and later the effects of changing temperature is analysed.

3.3.1 Frequency sweeps at constant temperature

The frequency response analysis is done by considering the system steady state response for a specific frequency. This analysis is done by two different ways: the first one starts the oscillations at different frequencies. After the steady state is reached, the system is stopped and then a new frequency is analysed. The second approach considers a sweep test around the resonant condition.

The forcing amplitude is set to be as high as physically possible in order to get as much as possible from the non-linearity of the SMA spring. There is a slight difference in the two experiments that are made, where the input amplitudes are 61 mm (0.94l_0) and 69 mm (1.06l_0) respectively, as seen in Fig. 11(a). This means that the amplitude of the forcing in the two experiments differ from each other. This results in different output amplitudes, a maximum of 55 mm (0.85l_0) and 68 mm (1.05l_0) respectively. However the qualitative behaviours in the two experiments are identical, the resonance frequency has not changed, which means that the difference in forcing amplitude is unimportant.

Fig. 11(a) presents the frequency response. This analysis points to a resonance frequency around 0.8 Hz (0.92ω_0) being associated with a non-symmetric peak. For frequencies just below the resonance the change in amplitude is very steep, which could indicate a jump in amplitude, and therefore coexisting attractors. Nevertheless, analysis of an up-sweep and down-sweep, shown in Fig. 11(b), does not show any sign of jumps in amplitude. Coexisting attractors have been observed experimentally in other SMA dynamical systems (Sitnikova *et al.* 2012). However, in

this case the hysteretic damping is too large, primarily because of pre-tension, to see such phenomena.

At this point, different sets of parameters are of concern. Fig. 12 shows the PE spring force and state space for three oscillator frequencies: below, at and above the resonance condition. The average stiffness of the PE spring is 24 N/m ($1.2k_0$) away from resonance and 18 N/m ($0.9k_0$) at resonance. It is important to observe that the system response during resonance is related to high amount of dissipation due to hysteresis. The equilibrium position changes within 5 mm ($0.08l_0$) with varying frequencies, which is in agreement with the movement of the equilibrium point investigated earlier.

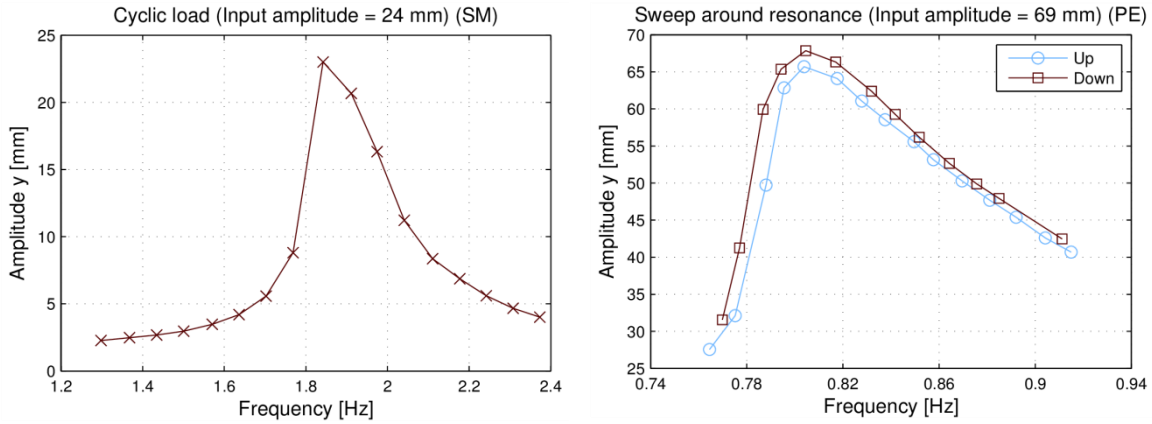

(a) (b)

Fig. 11 Frequency responses for the dynamical system with the PE spring

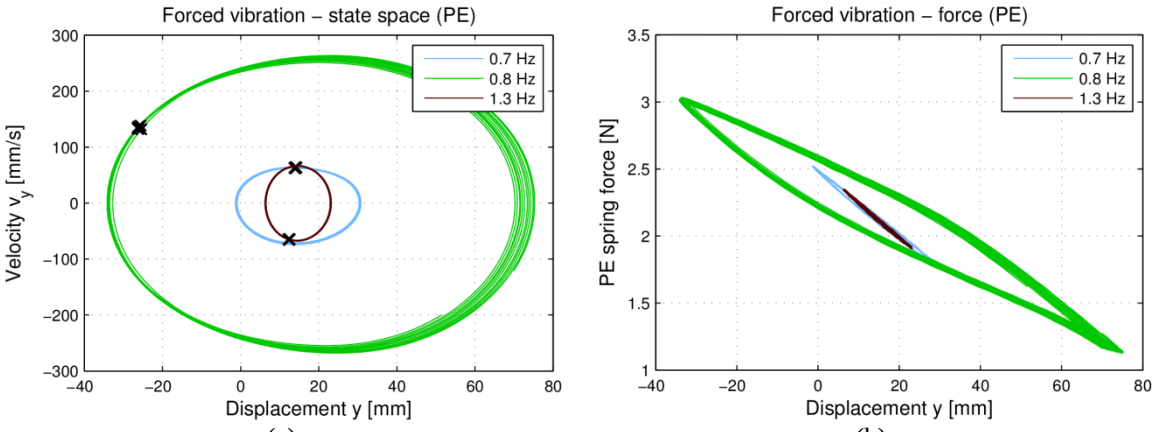

(a) (b)

Fig. 12 State space and PE spring force at several oscillator frequencies (below, at, and above resonance condition).The black crosses in (a) are Poincaré sections

3.3.2 Varying temperature

At this point, forced vibrations with temperature variations are investigated. This analysis is of special interest in terms of vibration reduction. The tests consider heating and cooling processes, defining two different conditions: hot and cold. Two forcing frequencies are evaluated. The analysis starts at room temperature (cold). After the steady state is reached the spring is heated (hot). When the new steady state is reached, the SMA spring is cooled to room temperature (cold). Results for these tests are shown in Fig. 13. The first frequency is very close to (and below) the resonance condition. The amplitude is 61 mm ($0.94l_0$) and the average stiffness is 17 N/m ($0.85k_0$). When the temperature is increased, the cart moves 61 mm ($0.94l_0$) to the right, the amplitude is decreased to 10 mm ($0.15l_0$) and the stiffness is increased to 37 N/m ($1.9k_0$). It is also worth mentioning that even though there is a lot of dissipation due to hysteresis in the low temperature case and none in the high temperature case the amplitude is lower in high temperature. Therefore, the change in amplitude is not a consequence of the change in dissipation that is counteracting, but due to the change in stiffness. The resonance frequency of the system is simply increased by heating the spring.

In the second case, the situation is the opposite. At low temperature the amplitude is 14 mm ($0.22l_0$) with an average stiffness of 24 N/m ($1.2k_0$). There is almost no hysteresis. When changing to high temperature the cart moves 63 mm ($0.97l_0$) to the right, the amplitude is increased to 47 mm ($0.72l_0$) and the stiffness is increased to 36 N/m ($1.8k_0$). The resonance frequency has moved closer. When the spring again becomes cold, the cart comes into the same steady state as before but oscillating around another point. The explanation for this is the same as for the similar free vibration results in Section 3.2.2. In cold condition the equilibrium is able to move almost arbitrarily and after the heating and cooling process, the system finds an equilibrium with the smallest possible martensite volume fraction in the PE spring.

4. Shape memory system

This section deals with the analysis of the SM system where a spring with shape memory effect is attached to the experimental set-up. The same analysis of the PE system is carried out, presenting a spring characterisation and then free and forced vibration investigations.

4.1 Spring characterisation

In order to characterise the SM spring, a DSC test is made. The results are presented in Fig. 14 and Table 3, showing the amount of heat per mass necessary to heat or cool the alloy with a constant temperature rate in time. At room temperature (25°C) the SM spring is in martensitic state since M_f is greater than room temperature.

The SM spring does not restore its initial length if subjected to an appropriate level of force without a heat treatment. Because of this, the SM system test is done differently from the one made for the PE system. Results of the force-displacement behaviour of the SM spring obtained in room temperature are shown in Fig. 15(a). The displacement path of one-fourth of the experiment follows the sequence O–A–B–C–B–C–B–C. After this, the spring is heated in order to get back to the original configuration. The test is repeated using a path with a new maximum displacement.

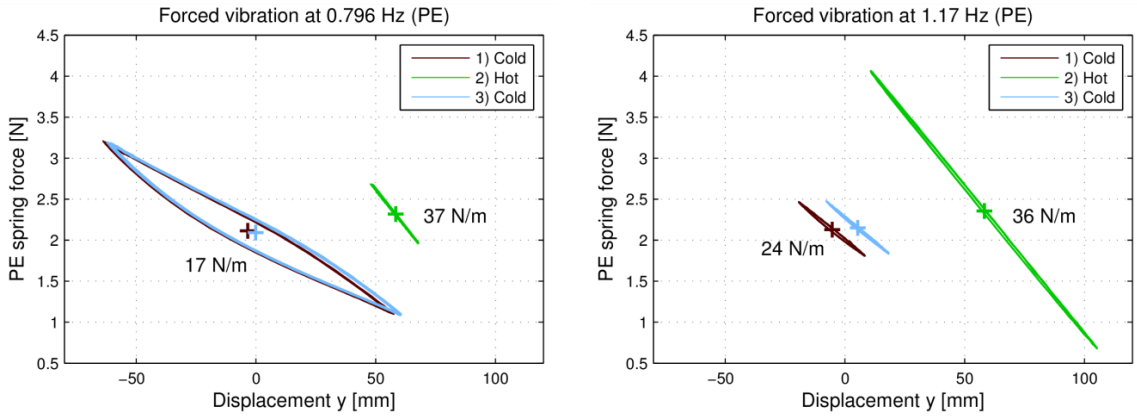

Fig. 13 Steady states at different temperatures for forced vibration of the system with the PE spring. It is heated with 1.0A. The plus signs indicate the respective equilibrium positions

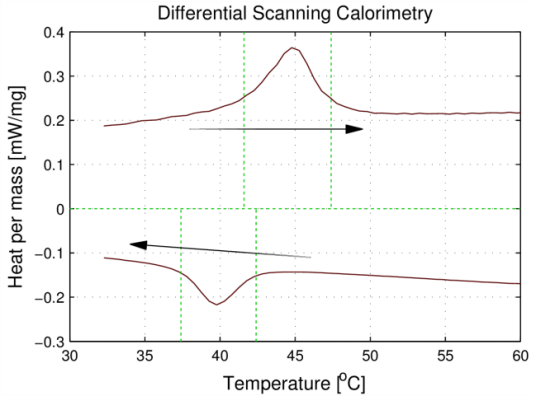

Fig. 14 The resulting graph from a DSC test for the SM spring

Table 3 Transformation temperatures for the SM spring extracted from the DSC test

M_f [℃]	37.4
M_s [℃]	42.4
A_s [℃]	41.6
A_f [℃]	47.4

The reorientation of the martensite in the spring starts around point A at 4 N ($3.1F_0$). The twinned martensite slope (O–A) is 67 N/m ($0.34k_0$). During the reorientation (A–F), the slope is 24 N/m ($0.12k_0$). The initial slope B–C is 160 N/m ($0.80k_0$), and the D–E slope is 210 N/m ($1.1k_0$). The difference in stiffness is the very same for F–G. For increasing tension, C–B, E–D and G–F, the slopes are almost constant and the same for the three, approximately 100 N/m ($0.50k_0$). This behaviour is consistent with the PE spring.

From these results the stiffness of the SM spring at room temperature is expected to vary within an interval of 100 to 210 N/m (a factor of two) or more as long as the pre-tension is higher than 60 mm ($3.2l_0$).

In higher temperatures, as seen in Fig. 15(b), the initial stiffness is increasing. This means that the austenitic shear modulus is higher than the one for twinned martensite. Also the transformations start at increasing stress levels. The slopes during transformations are almost the same for the three curves. Also in the heated cases, there are transformations back to twinned martensite/austenite, and in the 1.0 A case the spring is almost completely in the austenitic phase at the start, which results in almost no residual strain. A current of 1.0 A is estimated to be equivalent system set-up requires that the threads connecting the springs and the mass are in tension in all states, otherwise impact behaviour will influence the results. If the forcing is too high in this system, the threads become loose in some situations. Therefore the input amplitude is kept at an appropriately low level. E.g. at a pre-tension level of 3 N ($2.3F_0$) and a residual strain of 130 mm ($6.8l_0$) of the SM spring, cf. the midpoint of D–E in Fig. 15a, amplitudes cannot exceed approximately 25 mm ($1.3l_0$), because the SM spring then will reach point E, which is a tension-free state. Compared to the PE system, this means, that this system is much more restricted and only small forcing amplitudes where almost no phase transformation happens are possible.

4.2 Free vibration

Free vibration analysis is now in focus. The analysis is split into two parts: constant temperature and varying temperature.

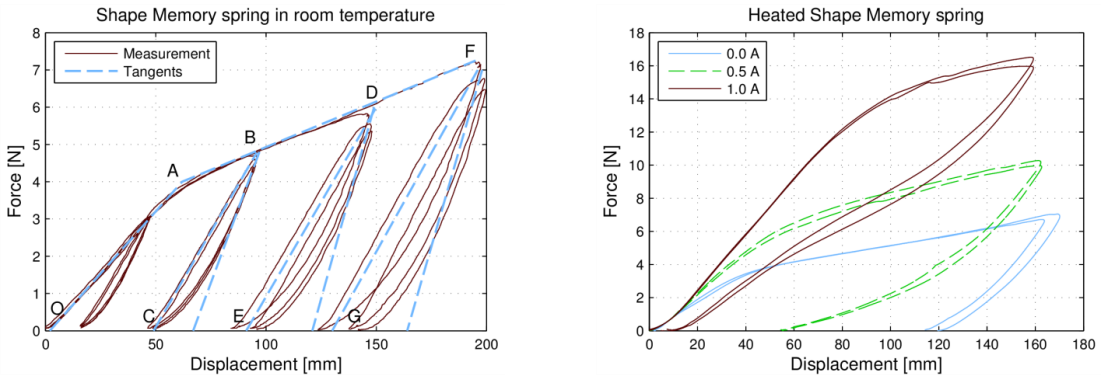

(a) (b)

Fig. 15 Force-displacement behaviour of the SM spring

4.2.1 Constant temperature

The analysis of the SM system is done by considering three different pre-stress levels at room temperature. The analysis of equilibrium points considers the 'equilibrium line' shown in Fig. 16, defined from the forces at the elastic spring F_E and SMA spring $F_{SMA} = F_{SM}$, when $F_{SM} = F_E$. The exact level of F_E is determined by the level of pre-stress.

The SM spring force and the state space for a pre-stress level of 2.9 N ($2.2F_0$) for the free vibration tests are shown in Fig. 17. Results are quite different from the PE system. Only the tests that start at y = 50 mm and y = 60 mm get through a phase transformation. For lower starting points the SM force slope is almost constant (approximately 195 N/m = $0.98k_0$), which is in agreement with the idea of identical stiffness for twinned and for detwinned martensite. Also these tests show that the cart is attracted to different equilibrium positions that are determined by the amount of detwinned martensite in the SM spring. Because of the lower amount of phase transformation, the dissipation levels are low.

Fig. 18 presents the equilibrium positions plotted as function of the starting points for three levels of pre-stress. To the left of the dashed line, the tendency is almost parallel to that line. This is because the average SM stiffness is constant as shown just before and that almost no phase transformation is taking place. This means that it is possible to change the equilibrium position more with the SM spring than with the PE spring using the initial stiffness as reference, and even more if it is seen relative to the maximum possible amplitudes.

4.2.2 Varying temperature

At this moment, temperature variations are of concern. In these tests, the cart is released at one of its equilibrium positions. Then the temperature is changed and the cart is moving due to the change in stiffness and also due to phase transformations in the SM spring. After heating, the spring is cooled down. A forced convection process is adopted employing a blower for the cooling process, see Fig. 1.

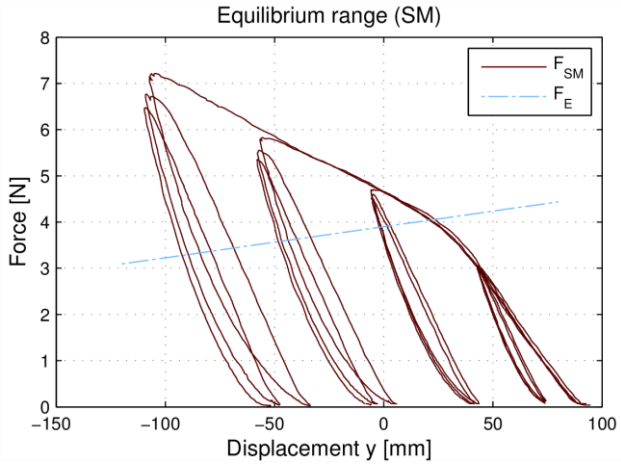

Fig. 16 Example of the range of equilibrium positions for the dynamical system with the SM spring

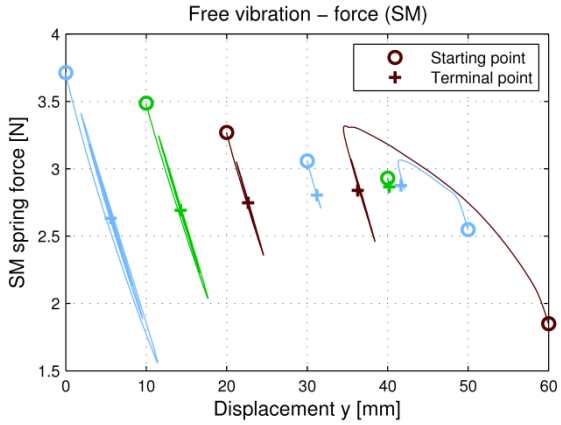

Fig. 17 SM spring force of seven free vibration tests with a pre-stress level of 2.9 N ($2.2F_0$)

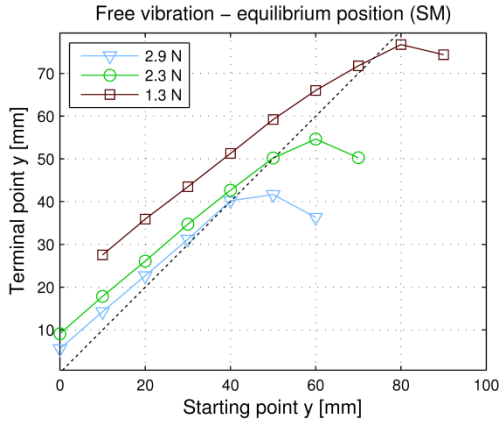

Fig. 18 Variation of equilibrium position for the SM system and 3 pre-stress levels. The starting point and terminal points are equal along the dashed line

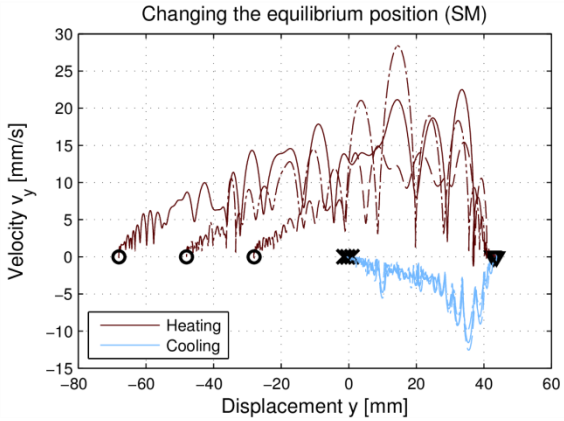

Fig. 19 The equilibrium position is changed due to temperature changes. The three different experiments start at ○, go to ▽ and end at ×

In Fig. 19 results are shown of the system at rest changing equilibrium position due to temperature variations. An indicative time constant for the heating process is 5 s, whereas for the cooling it is 7 s. Under these conditions, the SM system has similar behaviour when compared to the PE system. By heating the spring, it transforms into austenite and the residual strains due to phase transformation into detwinned martensite disappear. Likewise, the movement happens in a jagged fashion because of abrupt compliance due to phase transformation. The equilibrium position at this state is independent of the starting point. Therefore, Fig. 19 shows the triangles are placed on top of each other. When the spring is cooled down again the cart moves backwards, in a similar jagged fashion, but only to a minimum amount of detwinned martensite, which is also independent of the starting point. It is also important to observe that the state spaces for the three experiments are almost identical from the end of the heating process and during the cooling process for both types of springs. Note that the distance between the equilibrium positions are large compared to the initial length of the spring, see Table 1. The SM force is 3.9 N ($3.0F_0$) at $\bigtriangledown$ and 3.5 N ($2.7F_0$) at ×, which means that even though the spring is more elongated at × the spring force is less; this is the same as for the PE spring.

4.3 Forced vibration

Forced vibration analysis is now in focus by considering a sinusoidal excitation provided by a DC motor. Basically, it is presented the frequency sweeps analysis performed at constant temperature and then it is discussed the influence of temperature variations in system dynamics.

4.3.1 Frequency sweeps at constant temperature

The frequency analysis of the SM system is developed at room temperature. Fig. 20(a) presents the results and here it is seen that the resonance frequency is around 1.8 Hz ($0.89\omega_0$). The average stiffness of the spring is 200 N/m (k_0), which lie within the interval from 100 to 210 N/m obtained in Section 4.1. At the frequency sweep at room temperature, Fig. 20(b), the behaviour is identical to the PE spring. As seen the amplitude is marginally smaller on the up-sweep. This can be explained by the differences in initial conditions of detwinned martensite volume fraction that changes during the sweep. No amplitude jumps are detected like for the PE system. The SM system behaves close to linear as long as no phase transformations occur, and therefore it shows a close-to linear frequency response.

Fig. 21 shows the state space and force-displacement curves for three different situations: below, at and above the resonance. These results are similar to a linear system due to the low level of dissipation because almost no phase transformations are taking place. However, the average stiffness is decreased approximately 12% at the resonance.

4.3.2 Varying temperature

The analysis of forced vibration subjected to temperature variations is now in focus. Basically, two different frequencies are treated by considering a heating-cooling process. The system starts at a cold state, is heated and then cooled again. Force-displacement curves are presented in Fig. 22, showing three steady states: cold, hot and cold. The main difference between the two cases is that the system does not present great amounts of hysteresis, and the point around where the cart oscillates changes a lot more when compared to the amplitudes and stiffness.

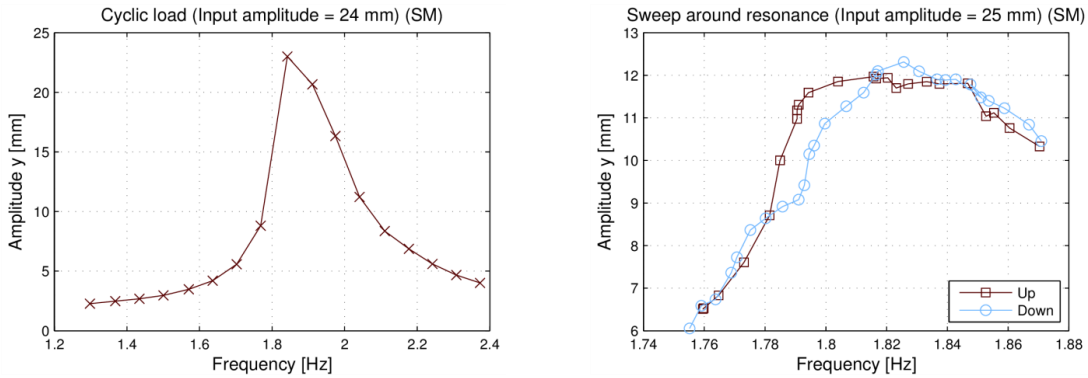

(a) (b)

Fig. 20 Frequency responses for the dynamical system with the SM spring

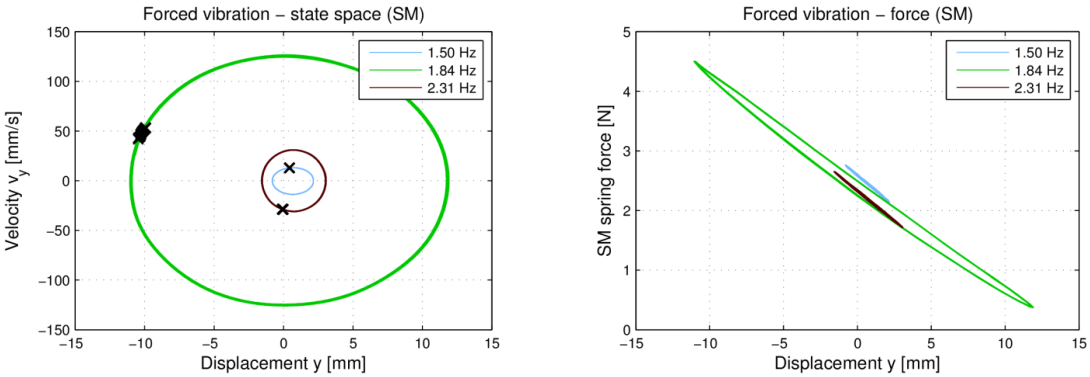

(a) (b)

Fig. 21 State space and SM spring force at several oscillator frequencies (below, at, and above resonance condition). The black crosses are Poincaré sections

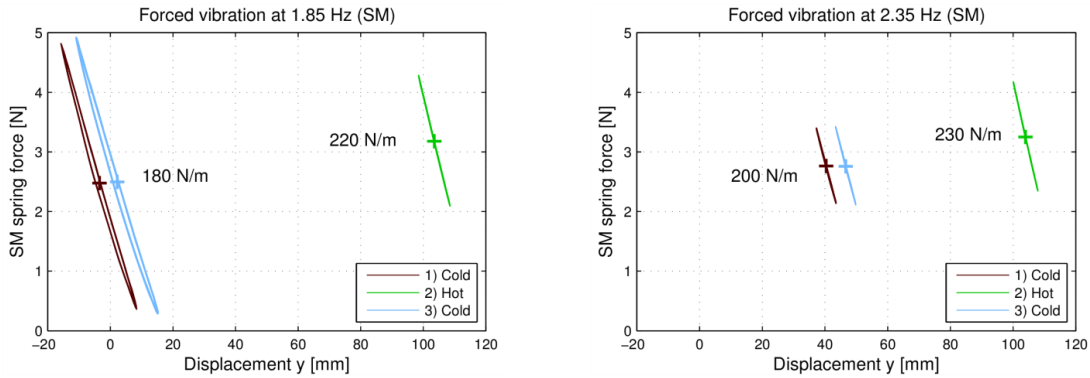

(a) (b)

Fig. 22 Steady state at different temperatures for forced vibration of the system with the SM spring. It is heated with 2.0A

At the low frequency, the average stiffness starts at 180 N/m ($0.9k_0$) and the amplitude is 12 mm ($0.63l_0$). There is a small amount of hysteresis. After heating the stiffness is increased to 220 N/m ($1.1k_0$) and the amplitude is decreased to 5 mm ($0.26l_0$). The point around where the cart oscillates has shifted 110 mm ($5.8l_0$). When the spring is cooled down again the cart settles at a marginally higher amplitude of 13 mm ($0.68l_0$) at higher y-values. Note that the force almost becomes zero in the cold cases.

At the high frequency, the oscillations start at higher y-values, since it is possible with these low amplitudes. The amplitude is increased slightly, from 3 mm ($0.16l_0$) to 4 mm ($0.21l_0$), when the spring is heated because of the change in average stiffness, from 200 (k_0) to 230 N/m ($1.2k_0$).

5. Conclusions

The non-linear dynamical response of SMA systems is investigated. The oscillator is composed by a cart connected to an elastic spring and to an SMA spring. A DC motor provides an external excitation to the system. Two distinct SMA springs are considered, defining two oscillators: pseudoelastic and shape memory.

Both of the dynamical systems are highly temperature dependent presenting a response defined by a competition between stiffness change and hysteretic behaviour. In general, pseudoelastic and shape memory systems have the capability to change the equilibrium positions due to temperature variations and large perturbations. In room temperature the pseudoelastic system can change the equilibrium position 50% of the initial length of the pseudoelastic spring, while it is 370% for the shape memory system. Changing from room temperature to a hot conditions the numbers are higher, namely 100% and 580% respectively. The changes in equilibrium positions for both systems happen in a jagged fashion because of abrupt compliance due to phase transformation.

The pseudoelastic system allows the use of high vibration amplitudes (e.g., 350% of initial spring length), dissipating great amounts of energy due to hysteretic response. This also means that the average stiffness of the spring decreases 25% at high vibration amplitudes, which result in a non-symmetric resonance peak in the frequency response. On the contrary, the shape memory system is restricted to low vibration amplitudes (130% of initial spring length), because of a requirement of remaining tension in the spring, which might be lost because of irreversible phase transformations at room temperature.

Temperature induced changes are essential in dynamical behaviour of SMA systems but has frequency constraints. For the pseudoelastic system it has been shown that an increase in temperature in the order of 50°C (estimated) is able to reduce vibration amplitudes up to 84% as consequence of a 120% increase in average stiffness of the spring at certain forcing conditions. For the shape memory system the average stiffness increases 20% resulting in a 58% decrease in vibration amplitudes in certain conditions.

SMAs have restrictions to be employed for active control because of generally slow temperature rates, but are strongly recommended for passive adaptive applications. Results show that changes in stiffness by temperature variations is effective to alter resonance conditions. Moreover, there is an extra change related to hysteretic response that is more effective at high amplitudes. Both behaviours establish a competition in order to define the system response.

Acknowledgements

The authors would like to thank the Danish Ministry of Science, Innovation and Higher Education for the support to the FTP Research project 12-127502, as well as the Brazilian Research Agencies CNPq, CAPES and FAPERJ and through the INCT-EIE (National Institute of Science and Technology - Smart Structures in Engineering) the CNPq and FAPEMIG for their support. The Air Force Office of Scientific Research (AFOSR) is also acknowledged.

References

Aguiar, R.A.A., Savi, M.A. and Pacheco, P.M.C.L. (2010), "Experimental and numerical investigations of shape memory alloy helical springs", *Smart Mater. Struct.*, **19**(2), 025008.

Aguiar, R.A.A., Savi, M.A. and Pacheco, P.M.C.L. (2013), "Experimental investigation of vibration reduction using shape memory alloys", *J. Intel.Mat. Syst. Str.*, **24**(2), 247-261.

Alam, M.S., Nehdi, M. and Youssef, M.A. (2008), "Shape memory alloy-based smart rc bridges: overview of state-of-the-art", *Smart Struct. Syst.*, **4**(3), 367-389.

Bernardini, D. and Rega, G. (2005), "Thermomechanical modelling, nonlinear dynamics and chaos in shape memory oscillators", *Math. Comput. Model.*, **11**(3), 291-314.

Casciati, S. and Hamdaoui, K. (2008), "Experimental and numerical studies toward the implementation of shape memory alloy ties in masonry structures", *Smart Struct. Syst.*, **4**(2), 153-169.

Casciati, S. and Marzi, A. (2010), "Experimental studies on the fatigue life of shape memory alloy bars", *Smart Struct. Syst.*, **6**(1), 73-85.

Dhanalakshmi, K., Avinash, A., Umapathy, M. and Marimuthu, M. (2010), "Experimental study on vibration control of shape memory alloy actuated flexible beam", *Int. J. Smart Sens. Intell. Syst.*, **3**(2), 156-175.

dos Santos, B.C. and Savi, M.A. (2009), "Nonlinear dynamics of a nonsmooth shape memory alloy oscillator", *Chaos Soliton. Fract.*, **40**(1), 197-209.

Lagoudas, D.C. (Ed). (2008), *Shape memory alloys: modeling and engineering applications*, Springer.

Lees, A.W., Jana, S., Inman, D.J. and Cartmell, M.P. (2007), "The control of bearing stiffness using shape memory", *Proceesings of the International Symposium on Stability Control of Rotating Machinery*.

Machado, L.G., Lagoudas, D.C. and Savi, M.A. (2009), "Lyapunov exponents estimation for hysteretic systems", *Int. J. Solids Struct.*, **46**(6), 1269- 1286.

Machado, L.G. and Savi, M.A. (2003), "Medical applications of shape memory alloys.", *Brazilian journal of medical and biological research Revista brasileira de pesquisas medicas e biologicas Sociedade Brasileira de Biofisica et al*, **36**(6), 683-691.

Nagaya, K., Takeda, S., Tsukui, Y. and Kumaido, T. (1987), "Active control method for passing through critical speeds of rotating shafts by changing stiffnesses of the supports with use of memory metals", *J. Sound Vib.*, **113**(2), 307- 315.

Ozbulut, O.E., Hurlebaus, S. and Desroches, R. (2011), "Seismic response control using shape memory alloys: A review", *J. Intel. Mat. Syst. Str.*, **22**(14), 1531-1549.

Paiva, A. and Savi, M.A. (2006), "An overview of constitutive models for shape memory alloys", *Math. Probl. Eng.*, **2006**, 1-30.

Phillips, J.W. and Costello, G.A. (1972), "Large deflections of impacted helical springs", *J. Acoust. Soc. Am.*, **51**(3), 967-973.

Savi, M.A., De Paula, A.S. and Lagoudas, D.C. (2011), "Numerical investigation of an adaptive vibration absorber using shape memory alloys", *J. Intel. Mat. Syst. Str.*, **22**(1), 67-80.

Savi, M.A. and Pacheco, P.M.C.L. (2002a), "Chaos and hyperchaos in shape memory systems", *Int. J. Bifurcat. Chaos*, **12**(3), 645-657.

Savi, M.A. and Pacheco, P.M.C.L. (2002b), "Chaos in a shape memory two-bar truss", *Int. J. Nonlinear Mech.*, **37**(8), 1387-1395.

Savi, M.A., Sá, M.A., Paiva, A. and Pacheco, P.M.C.L. (2008), "Tensile-compressive asymmetry influence on shape memory alloy system dynamics", *Chaos Soliton. Fract.*, **36**(4), 828-842.

Silva, L.C., Savi, M.A. and Paiva, A. (2013), "Nonlinear dynamics of a rotordynamic nonsmooth shape memory alloy system", *J. Sound Vib.*, **332**(3), 608-621.

Sitnikova, E., Pavlovskaia, E., Ing, J. and Wiercigroch, M. (2012), "Suppressing nonlinear resonances in an impact oscillator using smas", *Smart Mater. Struct.*, **21**(7), doi:10.1088/0964-1726/21/7/075028.

Sitnikova, E., Pavlovskaia, E., Wiercigroch, M. and Savi, M.A. (2010), "Vibration reduction of the impact system by an sma restraint: numerical studies", *Int. J. Nonlinear Mech.*, **45**(9), 837-849.

Song, G., Ma, N., Li, L., Penney, N., Barr, T., Lee, H.J. and Arnold, S. (2011), "Design and control of a proof-of-concept active jet engine intake using shape memory alloy actuators", *Smart Struct. Syst.*, **7**(1), 1-13.

Torra, V., Isalgue, A., Auguet, C., Carreras, G., Lovey, F.C., Soul, H. and Terriault, P. (2009), "Damping in civil engineering using sma. the fatigue behavior and stability of cualbe and niti alloys", *J. Mater. Eng. Perform.*, **18**(5-6), 738-745.

Williams, K., Chiu, G. and Bernhard, R. (2002), "Adaptive-passive absorbers using shape memory alloys", *J. Sound Vib.*, **249**(5), 835-848.

FC